OPEN

Sequential Path Entanglement for Quantum Metrology

Xian-Min Jin[1,2,3], Cheng-Zhi Peng[2], Youjin Deng[2], Marco Barbieri[3], Joshua Nunn[3] & Ian A. Walmsley[3]

[1]Department of Physics, Shanghai Jiao Tong University, Shanghai 200240, PR China, [2]Hefei National Laboratory for Physical Sciences at Microscale and Department of Modern Physics, University of Science and Technology of China, Hefei, Anhui 230026, PR China, [3]Clarendon Laboratory, University of Oxford, Parks Road, Oxford OX1 3PU, United Kingdom.

Path entanglement is a key resource for quantum metrology. Using path-entangled states, the standard quantum limit can be beaten, and the Heisenberg limit can be achieved. However, the preparation and detection of such states scales unfavourably with the number of photons. Here we introduce sequential path entanglement, in which photons are distributed across distinct time bins with arbitrary separation, as a resource for quantum metrology. We demonstrate a scheme for converting polarization Greenberger-Horne-Zeilinger entanglement into sequential path entanglement. We observe the same enhanced phase resolution expected for conventional path entanglement, independent of the delay between consecutive photons. Sequential path entanglement can be prepared comparably easily from polarization entanglement, can be detected without using photon-number-resolving detectors, and enables novel applications.

Q uantum metrology, which harnesses the collective nature of entangled particles, is an emerging technology that promises to revolutionise our way of measuring and to radically alter the limits for parameter estimation[1–4]. The most common example, which is also the one with the most technological applications, is the estimation of the relative optical phase between two arms of an interferometer: this problem is directly related to the realization of atomic clocks[5], the investigation of biological samples[6], and the detection of gravitational waves[7,8]. Generating light in an entangled state delocalised over the two arms can achieve a better scaling of the precision with the number of photons than is possible with any classical optical technique. Indeed, for a classical coherent state with average photon number N, the precision in phase estimation will mostly be limited by the Poissonian fluctuations of the photon number, the so-called *shot noise*, which contributes a scaling proportional to $1/\sqrt{N}$ on the error of the phase estimate (this is the 'standard quantum limit'). In the quantum domain N photons can be prepared in an entangled superposition of all photons occupying one arm, and of all photons occupying the other arm. Since all photons travel together, phase is accumulated more rapidly, which allows for a phase estimate with enhanced precision whose error scales as $1/N$, the Heisenberg limit[9].

The key elements for realising such an advantage are the ability to produce N-photon path-entangled states, and the capability of resolving the number of photons at both output ports of the interferometer. However, scaling up from the few-photon level has proven to be technically challenging, since the best photon sources available produce multiphoton states with unwanted components, which degrades the quantum advantage[10–16]. This motivates research into less technically demanding schemes that might retain the enhanced precision of conventional path-entangled states. Here we propose breaking up N-photon entangled states so that the entangled photons are distributed over N time bins, with only one photon interacting with the sample at a time. This type of *sequential path-entangled* (SPE) state has a number of advantages. First, as we will show, SPE states can be produced directly from Greenberger-Horne-Zeilinger (GHZ) states[17]; the current state of the art for producing GHZ states[18,19] is more advanced than for $N00N$ states[15,16], so that larger SPE states can be synthesised than $N00N$ states. Second, detecting photons one at a time can be done with conventional avalanche photodetectors without requiring photon-number-resolving detection. Finally, SPE states sample a phase over a range of times, which enables the extraction of Fourier components of a dynamical phase.

A legitimate concern with a proposal to break up and separately detect an entangled state in this way is that the metrological power of a collective measurement on the entangled state is lost. However it is known that strategies based on collective measurements offer no advantage for quantum metrology[1], and this is why SPE states can be just as powerful for metrology as conventional path-entanglement. In this paper we demonstrate the key features of this proposal by recording the interference produced by two-photon entangled states as a time delay between the photons is introduced. The results show that phase super-resolution is maintained independent of the delay,

confirming the power of SPE states as a resource for quantum metrology. We generate our SPE states by feeding a polarization-entangled photon pair into a modified Mach-Zehnder interferometer[20] (MZI). More generally, we establish that higher order SPE states could be deterministically produced from an initial resource of GHZ polarization-entangled states by means of optical switching.

Results

Sequential path entanglement. The archetypal path-entangled state is the N00N state[3,21], $|N0::0N\rangle = |N\rangle_a|0\rangle_b + e^{iN\phi}|0\rangle_a|N\rangle_b$ (ignoring normalisation here, and below), in which N photons are superposed between all propagating in one arm, a, of an MZI, and all propagating in the other arm b (see Fig. 1 (a)), which accrues a phase rotation $N\phi$, where ϕ is the relative phase between the two arms of the MZI. The advantage of this path-entangled state for metrology can be understood using the concept of the photonic *de Broglie wavelength*[22]. The N photons are treated as an effective single entity, and thus have an effective de Broglie wavelength λ/N, with λ the single-photon wavelength.

The scheme that is most commonly used to produce approximate N00N states is shown in Fig. 1 (a). Two Fock states $|N/2\rangle$ are made to interfere on the first beam splitter (BS) of an MZI. For $N = 2$, Hong-Ou-Mandel (HOM) interference[23] directly generates the required photon-bunched $|20::02\rangle$ state[16,24]. Unfortunately, for $N > 2$, generating a genuine N00N state by HOM interference in this way no longer works: the resulting state is instead a superposition of $|N0::0N\rangle$ with an undesired contribution $|\Omega(N)\rangle$, which decreases the associated measurement precision[13,25,26]. For instance, Nagata *et al.* prepared a 4-photon N00N state with $|\Omega(4)\rangle \propto |22\rangle$, by interfering 2-photon Fock states[13]. States of this form are known as

Holland-Burnett[27] states, and, while they are interesting for lossy phase estimation[28], they cannot achieve the Heisenberg limit. It has been proposed that $|\Omega(N)\rangle$ can be suppressed by using feedforward[29], however, this proposal has not been implemented yet.

Multiphoton SPE states can be generated without suffering from the complications described above that make N00N states difficult to produce for $N > 2$. We begin with a polarization-entangled GHZ state[18,19] of N photons,

$$|\text{GHZ}(N)\rangle = |H\rangle_1|H\rangle_2 \ldots |H\rangle_N + |V\rangle_1|V\rangle_2 \ldots |V\rangle_N, \quad (1)$$

in which $|H\rangle_i$ ($|V\rangle_i$) denotes a horizontally (vertically) polarized photon in spatial mode $i = 1, 2, \ldots, N$. The conversion of this GHZ state into an SPE state is schematically shown in Fig. 1 (b). Each photon from the GHZ state is delayed with respect to the next and then all are transferred into a single spatial mode. In our experiments we combine the photons probabilistically, using a beam splitter, but in general this step could be done *deterministically* by means of a fast optical switch, such as a Pockels cell[30]. Finally, path entanglement is created by directing the photons one by one onto a polarizing beam splitter followed by a half-wave plate at one output mode, which applies the operation $|H\rangle \rightarrow |1\rangle_a|0\rangle_b$; $|V\rangle \rightarrow |0\rangle_a|1\rangle_b$. This recipe allows the deterministic conversion of GHZ entanglement into SPE states within the MZI of the form

$$|\text{SPE}(N)\rangle = \prod_{j=1}^{N} |1\rangle_{a,t_j}|0\rangle_{b,t_j} + \prod_{k=1}^{N} |0\rangle_{a,t_k}|1\rangle_{b,t_k}, \quad (2)$$

where now each temporal mode t_j contains a single path-entangled photon. Each of the N photons in mode b picks up the interferometer phase ϕ, and so this state also exhibits super-resolution, like the N00N state (see Methods). However, the time separation of the
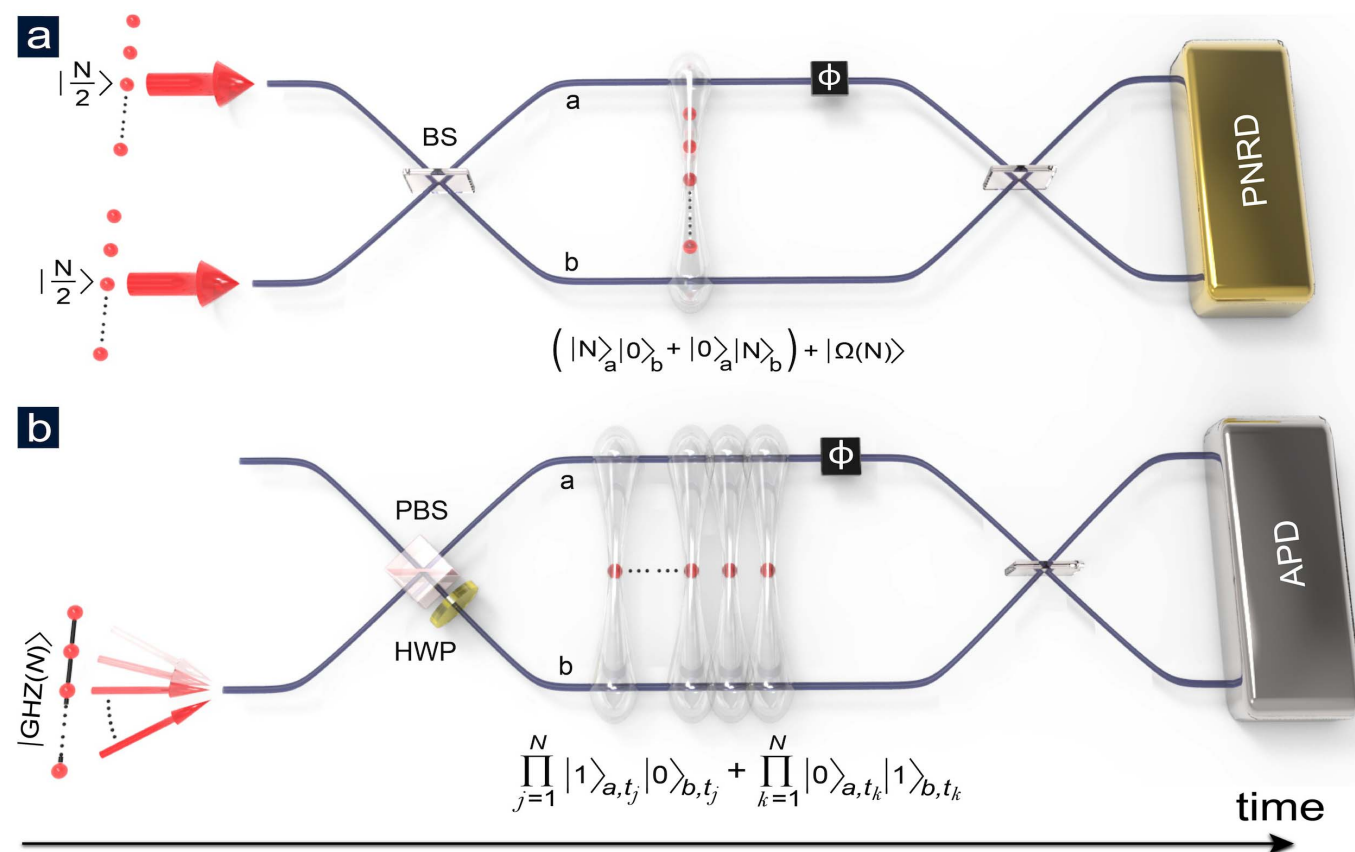

Figure 1 | Preparation of N00N states and SPE states. (a) Approximate preparation of N00N states by interfering Fock states. (b) Deterministic preparation of SPE states converted from polarization-entangled GHZ states in a sequential way. BS: beam splitter; PBS: polarizing beam splitter; HWP: half-wave plate; APD: avalanche photodetectors; PNRD: photon-number-resolving detectors; ϕ: phase shift.

photons means that photon-number resolving detectors are not required to identify the N-photon events containing the enhanced metrological signal. In principle, 'on-off' detectors such as commercially-available avalanche photodetectors can be used, since there is only a single particle in each time bin[31]. Additionally, if the MZI phase is varying in time — as would be typical in pump-probe type experiments — the Fourier components of the phase evolution can be accessed efficiently via the transmission statistics of SPE states by tuning the time delay $T = t_{j+1} - t_j$ into resonance with a component of interest (see Methods).

Experimental setup. Our experiment is shown schematically in Fig. 2. It contains two parts: the photon source (Fig. 2 (a)) which produces polarization-entangled photon pairs, and the modified MZI (Fig. 2 (b)). In the experiment, as shown in Fig. 2 (a), type-II spontaneous parametric down conversion[32] (SPDC) is employed to generate a polarization-entangled state $|H\rangle_{P_1}|H\rangle_{P_2} + |V\rangle_{P_1}|V\rangle_{P_2}$ (see Methods). A translation stage with μm precision adds an adjustable delay ΔL_1 into path P_1, and then P_1 and P_2 are combined at a 50:50 beam splitter BS1 and the resulting polarization-entangled state is coupled into an optical fibre in mode P_4 for delivery to the MZI. We note that BS1 passively combines the photons into the same spatial mode in a probabilistic way, which allows us to study several delay settings, including $\Delta L_1 = 0$. But for a sufficiently large delay $\Delta L_1 \gg \xi$, where ξ is the single photon coherence length, the photons are well-separated and could be deterministically combined using a fast optical switch, allowing the efficient conversion of higher-photon-number GHZ states into SPE states. The state emerging from the fibre is converted into an SPE state of the form (2) at a polarizing beam splitter, and a nm-precision piezoelectric actuator mounted on

a μm-precision translation stage is used to control the optical path length difference ΔL_2 within the modified MZI.

To find the position $\Delta L_2 = 0$ we first maximise the visibility of single-photon interference in the MZI (see Fig. 2 (d)). For these measurements BS1 is replaced by a polarizer oriented at 45°, so that photons emitted from the source into path P_1 are delocalised at the polarizing beam splitter, producing a fringe pattern in the singles count rates recorded in the paths P_7, P_8, as ΔL_2 is scanned (photons in path P_2 are simply dumped). The full width at half maximum of the pattern provides a measurement of the single-photon coherence length $\xi \approx 130 \; \mu m$, consistent with the result deduced from the measured HOM interference dip shown in Fig. 2 (c) (see Methods). We then set $\Delta L_2 \approx 0$ and scan the piezoelectric actuator in steps of 10 nm to observe the fringe spacing, which matches the single photon de Broglie wavelength (simply the optical wavelength) $\lambda \approx 810 \; nm$ (see Fig. 3 (a)).

Next, we verify phase super-resolution with a standard $N00N$ state by setting $\Delta L_1 = 0$, so that both photons emitted from the source are temporally overlapped in the MZI. As shown in Fig. 2 (e), the coincidence count rate at detectors D_1 & D_2 exhibits an interference pattern with a broader envelope than the single photon interference pattern. This is due to spectral entanglement of the photon pairs emitted by our source, which introduces temporal correlations that are limited only by the coherence time of the downconversion pump laser, extending significantly beyond the single-photon coherence time (see Methods for details). We comment that to our knowledge this is the first time the extended interference pattern of a $|20::02\rangle$ state generated with a spectrally anti-correlated photon pair source has been fully mapped out[24]. The fine-grained scan of the region around $\Delta L_2 = 0$ in Fig. 3 (b) shows the expected half-period fringes
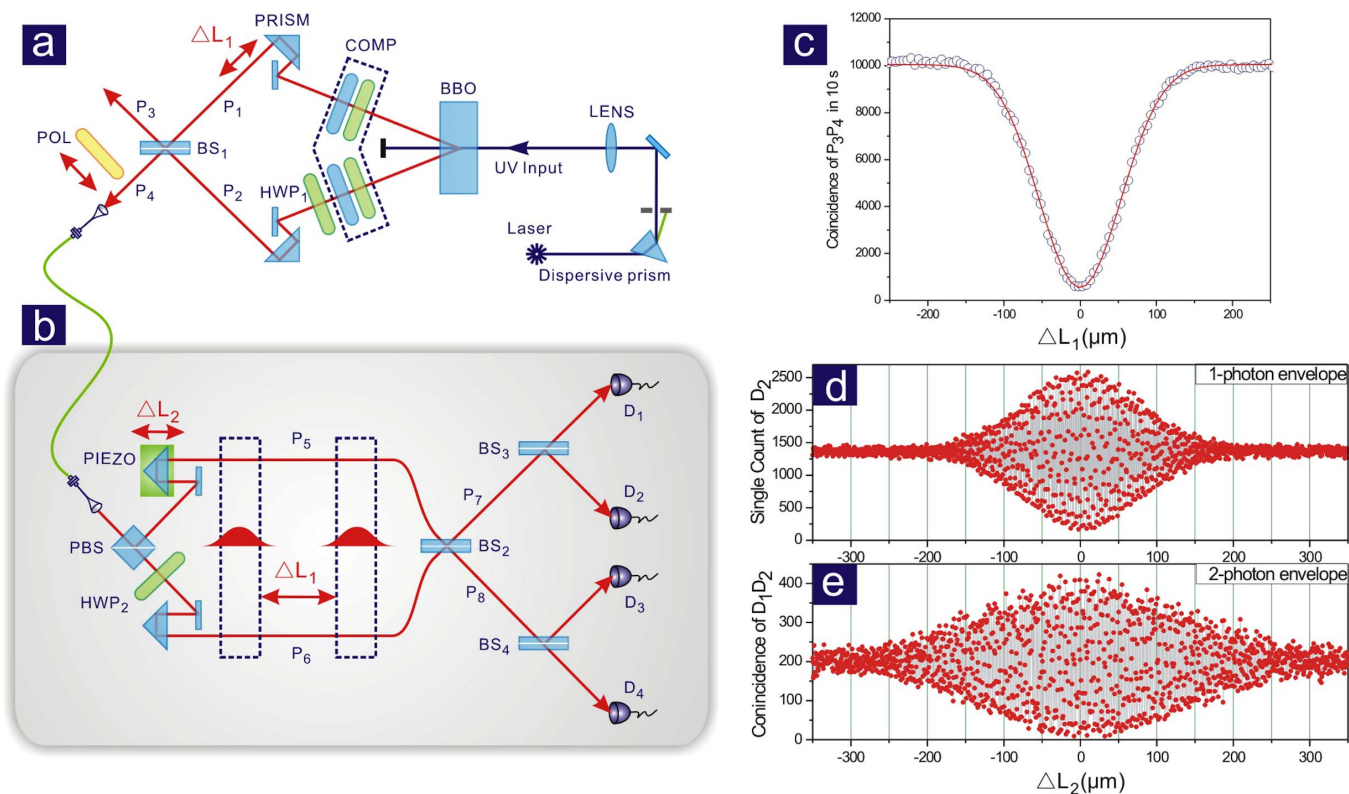

Figure 2 | Schematic experimental setup and one- and two-photon interference. (a) Preparation of coaxial polarization-entangled state. Polarization entangled photon pairs are generated by type II degenerate SPDC in a nonlinear crystal. BS1 serves as a probabilistic optical mixer coupling both entangled photons into path P_4. ΔL_1 is tuned by scanning the position of a prism mounted on a translation stage. (b) A modified MZI. (c) The two-photon coincidence rate measured in paths P_3 and P_4 exhibits a characteristic dip as ΔL_1 is scanned, indicative of HOM interference at BS1. (d), (e) One- and two-photon interference patterns. BBO: β-barium-borate crystal; COMP: HWP and BBO (1 mm); POL: polarization plate; PIEZO: piezoelectric actuator.
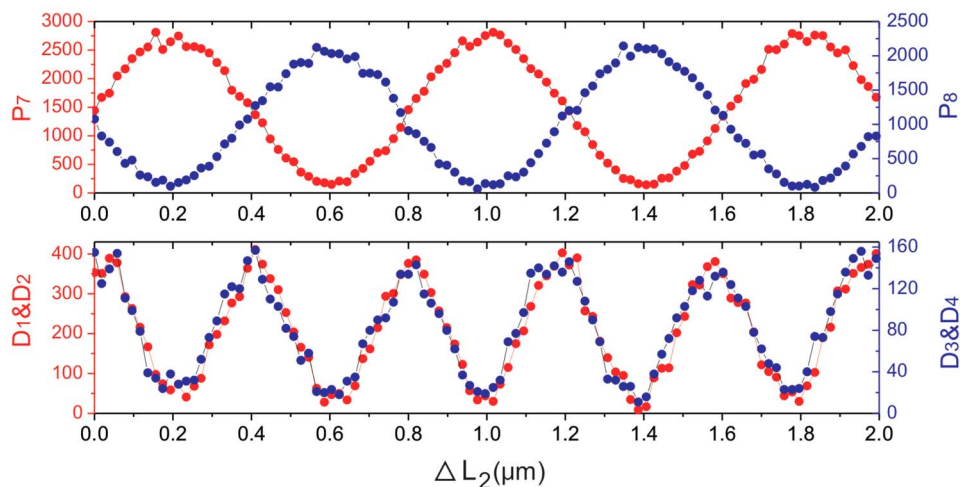
Figure 3 | Characteristics of one- and two-photon interference. (a) Single-photon count rate in path P_7 (red solid circles) and at P_8 (blue solid circles) as the delay ΔL_2 is varied. Both output modes of the interferometer are directed to similar detection set-ups, which provides a consistency check. (b) Two-photon coincidence rates at detectors D_1, D_2 (red solid circles) and at detectors D_3, D_4 (blue solid circles) versus ΔL_2; events with a time separation within $\Delta L_1/c$ are considered as coincident.

associated with the reduced de Broglie wavelength of the $|20::02\rangle$ state.

Independence of the separation between photons. To verify that SPE states have the same reduced de Broglie wavelength as the $N00N$ state, independent of the delay between successive photons entering the MZI, we carried out experiments for $\Delta L_1 = 200$ μm and 10,000 μm. The setting $\Delta L_1 = 200$ $\mu m > \xi$ is larger than the single-photon coherence length but still less than the coherence length of the pump laser $\xi_{\mathrm{pump}} \approx 300$ μm, while $\Delta L_1 = 10,000$ μm is significantly larger than ξ_{pump}. Fig. 4 shows the

interference patterns in the coincidence rates for detectors D_1 and D_2 produced by scanning ΔL_2. For each of the scans, the periodicity is always about 405 nm, half of the single-photon wavelength $\lambda = 810$ nm, which confirms that SPE states retain the phase super-resolution of a conventional $N00N$ state, even when consecutive photons are separated well beyond their individual coherence lengths. It is clear that the coincidence rates fall as ΔL_1 is increased, but this simply represents a reduction in the SPE preparation efficiency. This is because for $\Delta L_1 < \xi$, HOM interference at BS1 boosts the probability that photon pairs are coupled into our MZI, whereas for $\Delta L_1 \gtrsim 150$ μm there is no longer HOM

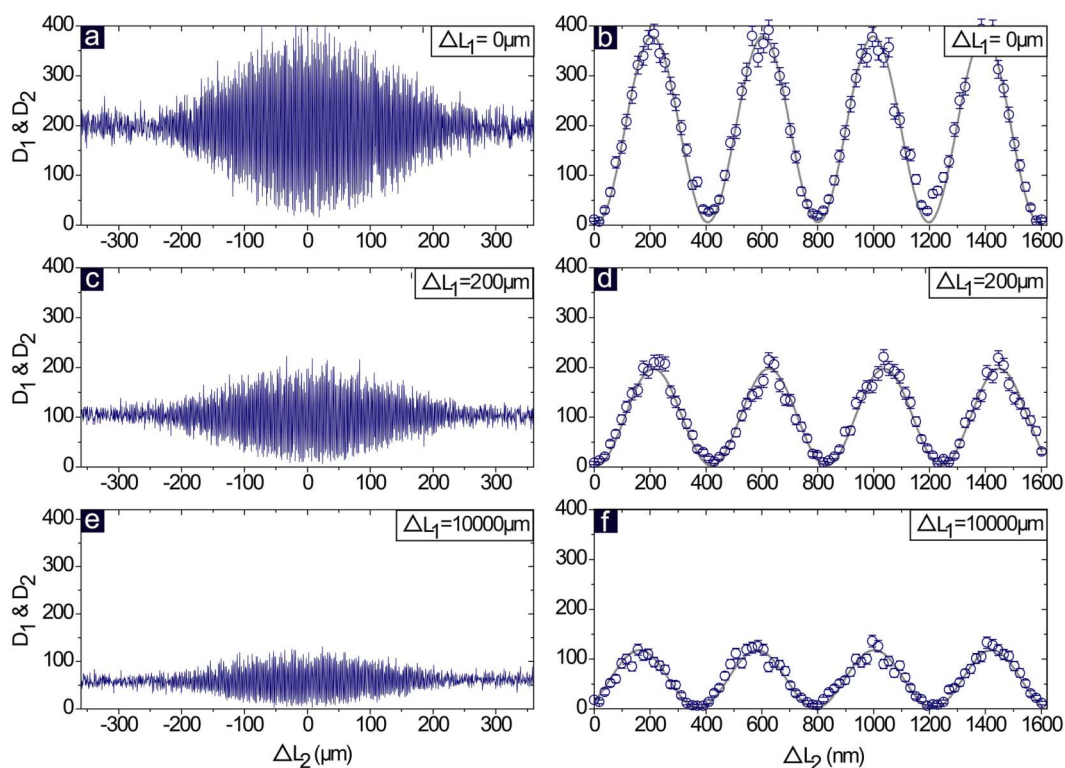**Figure 4 | Two-photon interference envelope and fringes versus interval ΔL_2.** Error bars are given by Poissonian statistics. (a), (b) $\Delta L_1 = 0$ μm. (c), (d) $\Delta L_1 = 200$ μm. (e), (f) $\Delta L_1 = 10,000$ μm.

interference. In addition, the fibre coupling efficiency drops for large ΔL_1. In particular, the setting $\Delta L_1 = 10{,}000\ \mu m$ exceeds the Rayleigh range defined by our fibre, causing a significant drop in the coincidence rate for this measurement. However, the peak visibilities of the patterns in parts (b)–(f) of Fig. 4 remain high throughout the scan, at 0.98 ± 0.01, 0.95 ± 0.03 and 0.98 ± 0.03, respectively. From this we conclude that the quality of the bi-photon interference is independent of ΔL_1, and the reduced photonic de Broglie wavelength is independent of the distance between photons in an SPE state.

Discussion

We have introduced SPE states as an alternative resource for quantum-enhanced optical interferometry. Conventional $N00N$ states are difficult to produce, and photon-number-resolving detectors[33–35] are required to extract a metrological signal[36]. While multiplexed on-off detectors can be realized easily, they only count photon number approximately, and are therefore not suitable for metrological applications. By contrast, SPE states can be generated deterministically from GHZ states, which are easier to produce than $N00N$ states. Photon-number-resolving detectors are also not needed, since photons can be detected sequentially[1]. In practice, the performance of photodetectors is critical to achieving a metrological advantage with $N00N$ states[28], and this remains the case for SPE states also. However, realistic quantum interferometry could be realised using recently developed highly efficient, fast, detectors[37].

Many experiments have shown that two photons arriving simultaneously make a substantial difference in second harmonic generation[38], Kerr-like interactions[39] and Rydberg atomic gases[40]. This detrimental effect makes phase estimation modeling complicated. Furthermore, quantum metrology is often motivated by the need to probe refractive index variations in samples with extreme sensitivity to optical radiation[41]. $N00N$ states can excite 2-photon or multiphoton transitions in a sample that scatter light out of the interferometer, and such transitions can ionise quantum systems and damage biological molecules. The influence of multiple photons will become stronger if more photons are present at one time, as could be the case with high-N $N00N$ states, which are the ultimate goal of this avenue of research. By contrast even large-N SPE states can excite only single-photon transitions because the constituent photons arrive one at a time.

It is also notable that SPE states can be used to extract the harmonic spectrum of a time-varying phase: if the consecutive time bins in an SPE state are separated by a constant delay T, the phase is sampled periodically, producing a signal proportional to the amplitude of the Fourier component of the dynamical phase at a frequency $f = 1/T$ (see Methods).

We experimentally confirmed that 2-photon SPE states posses the same phase super-resolution as 2-$N00N$ states. Unlike schemes for achieving super-resolution via post-selection on classical light[42], this super-resolution is of quantum origin, and SPE states therefore represent a convenient and powerful platform for quantum-enhanced phase sensing via optical interferometry.

Methods

Preparation of polarization-entangled photonic source. As shown in Fig. 2 a CW semiconductor laser produces a blue beam (power 34.5 mW, waist 100 μm, central wavelength 405 nm) that pumps type-II degenerate SPDC in a 2 mm β-barium-borate (BBO) crystal, producing pairs of photons with central wavelength 810 nm[32]. The down-converted signal and idler photons have different propagation velocities and travel along different paths inside the crystal due to its birefringence. The resulting walk-off effects are compensated by a combination of a half-wave plate and a 1 mm BBO crystal in each arm. Photons are then coupled into single mode fibres and we prepare a polarization-entangled state $|H\rangle_{P_1}|V\rangle_{P_2} + |V\rangle_{P_1}|H\rangle_{P_2}$. The state is further transformed to be $|H\rangle_{P_1}|H\rangle_{P_2} + |V\rangle_{P_1}|V\rangle_{P_2}$ by placing a half-wave plate with 45° in mode P_2. The singles count rates measured directly in each of P_1, P_2 are about 80,000 per second, and the coincidence rate is about 20,000 pairs per second. The visibilities for the polarization correlations are about 98% in the $|H\rangle/|V\rangle$ basis and 93%

for the $|+45^\circ\rangle/|-45^\circ\rangle$ basis. This shows that we have produced a high-quality polarization-entangled photonic source.

Success rate for combination of photon pairs at BS1. When $\Delta L_1 \gtrsim \xi$, the photons do not overlap at BS1 and each photon has the same probability to be transmitted or reflected. Thus, the photon state in P_4 can be a single-photon state $|H\rangle$ or $|V\rangle$ with probability 0.25, respectively, or the maximally polarization-entangled state $|\psi\rangle$ with probability 0.25 (the rest of the time, P_4 contains no photons). When $\Delta L_1 < \xi$, HOM interference suppresses the single photon probabilities, boosting the probability for coupling both photons into P_4 up to 1/2 for $\Delta L_1 = 0$. HOM interference with a visibility of $94.5 \pm 0.4\%$ is shown in Fig. 2 (c), obtained by scanning ΔL_1 and measuring the coincidence rate at two output modes P_3 and P_4 (Fig. 2 (c)). The high visibility certifies good spatial and temporal overlap for the entangled photon pairs emitted by our source. A Gaussian fit to the HOM dip in Fig. 2 (c) yields the single-photon coherence length $\xi \approx 126\ \mu m$.

Single- and bi-photon coherence time. Here we briefly outline the origin of the differing widths of the single and bi-photon interference patterns shown in parts Fig. 2 (d) and (e). We consider that our downconversion source creates photon pairs in the entangled state

$$|\psi\rangle = \int \zeta(\omega,\omega')|\omega + \omega_0, \omega' + \omega_0\rangle\, d\omega d\omega',$$

where ζ is the joint spectral amplitude for emitting signal and idler photons with frequencies $\omega + \omega_0$, $\omega' + \omega_0$, with ω_0 the centre frequency of the downconversion. ζ generally extends over a broad bandwidth set by the phasematching conditions in the downconversion crystal, but energy conservation enforces tight frequency anti-correlations, with a correlation width equal to the pump laser bandwidth.

For the single photon interference measurement (Fig. 2 (d)) we dump photons P_2, leaving the photons in P_1 in the mixed state $\rho = \iint f(\omega_1,\omega_2)|\omega_1 + \omega_0\rangle \langle\omega_2 + \omega_0| d\omega_1 d\omega_2$, where $f(\omega_1,\omega_2) = \int \zeta(\omega_1,\omega)\zeta*(\omega_2,\omega) d\omega$, The MZI implements the transformation

$$\rho \rightarrow \rho' = \iint f(\omega_1,\omega_2)\left[1 \pm e^{i(\omega_1 + \omega_0)\Delta L_2/c}\right]\left[1 \pm e^{-i(\omega_2 + \omega_0)\Delta L_2/c}\right]$$
$$|\omega_1 + \omega_0\rangle\langle\omega_2 + \omega_0| d\omega_1 d\omega_2$$

at the two output ports P_7, P_8 (postselected on no photon in the other port), and the single photon count probability is $P = \mathrm{tr}\left\{\rho' \int d\omega |\omega\rangle\langle\omega|\right\} = \int p(\omega)\left|1 \pm e^{i(\omega + \omega_0)\Delta L_2/c}\right|^2 d\omega$, where $p(\omega) = f(\omega,\omega)$ is the marginal spectrum. This exhibits fringes with period $\lambda = 2\pi\omega_0/c$ and visibility V given by a Fourier transform, $V(\Delta L_2) = \mathcal{F}_\omega\{p(\omega)\}(\Delta L_2/c)$, so that the coherence length ξ is determined by the inverse of the bandwidth of $p(\omega)$. Note that the fringe patterns for the two output ports are π out of phase, as seen in Fig. 3 (a).

For the measurement of the two photon $N00N$ state interference (Fig. 2 (e)), the MZI produces the state

$$|\psi'\rangle = \iint \zeta(\omega,\omega')\left[1 + e^{i(\omega + \omega' + 2\omega_0)\Delta L_2/c}\right]|\omega + \omega_0, \omega' + \omega_0\rangle d\omega\, d\omega'$$

at each of its two output ports (postselected on no photons in the other port). The coincidence probability at detectors D_1, D_2 is then $\mathcal{P} = \mathrm{tr}\left\{|\psi'\rangle\langle\psi'| \iint d\omega\, d\omega'|\omega,\omega'\rangle\langle\omega,\omega'|\right\}$, which produces an interference pattern with period $\lambda/2$ and visibility given by $V(\Delta L_2) = g(\Delta L_2/c, \Delta L_2/c)$, where $g(t,t') = \mathcal{F}_{\omega,\omega'}\left\{|\zeta(\omega,\omega')|^2\right\}(t,t')$ is the two-dimensional Fourier transform of the joint spectral intensity $|\zeta(\omega, \omega')|^2$. The tight frequency anti-correlations between the photons produce strong temporal correlations such that the width of $g(\Delta L_2/c, \Delta L_2/c)$ is proportional to the coherence length ξ_{pump} of the pump laser.

Super-resolution with SPE states. To convert $N00N$ states into SPE states we simply introduce a delay ΔL_1 between photons, which for the bi-photon case corresponds to the transformation $\zeta(\omega,\omega') \rightarrow \zeta(\omega,\omega')e^{i(\omega' + \omega_0)\Delta L_1/c}$. However, as described above, the bi-photon interference visibility depends only on the joint spectral intensity, which is unaffected by this phase rotation. This is why our SPE state retains phase super-resolution for all values of ΔL_1. For higher photon number states with $N > 2$ the visibility is determined by higher order correlation functions, but the coincidence rate is always invariant under phase rotations of the joint spectrum, so that the metrological power of SPE states is independent of the delay between photons.

Extracting dynamical phase information with SPE metrology. An interesting feature of SPE states is that the photons sample the MZI phase over a set of discrete times t_j, meaning that the metrological signal is of the from $V\cos^2(\Phi)$, where V is a visibility, and where $\Phi = \sum_{j=1}^{N} \phi(t_j)$. Substituting in the Fourier relation $\phi(t) = (2\pi)^{-1/2}\int \tilde{\phi}(\omega)e^{i\omega t} d\omega$, where $\tilde{\phi}$ is the spectrum associated with the time-varying phase (note that here ω is the Fourier conjugate of t, and not an optical frequency), we obtain

$$\Phi = \int \Delta(\omega)\tilde{\phi}(\omega) d\omega; \quad \Delta(\omega) = (2\pi)^{-1/2}e^{i\omega t_0}e^{i(N-1)\omega T/2}\frac{\sin(N\omega T/2)}{\sin(\omega T/2)}, \quad (3)$$

where we assumed a constant inter-photon delay $t_j = t_0 + (j-1)T$ (in our experiment we had $T = \Delta L_1/c$). The function Δ comprises a series of spectral peaks of height

$(2\pi)^{-1/2}e^{i\omega_k t_0}$, located at the frequencies $\omega_k = 2\pi k/T$; $k = \ldots, -2, -1, 0, 1, 2, \ldots$, each with width $\delta\omega = 4\pi/NT$. In the limit that N is large, we may approximate Δ as a series of Dirac delta functions, so that the SPE signal can be written as

$$\Phi \propto \sum_{k=-\infty}^{\infty} e^{-i\omega_k t_0}\tilde{\phi}_k. \qquad (4)$$

We would like to extract information about the Fourier components $\tilde{\phi}_k = \tilde{\phi}(\omega_k)$ of the phase; as an example we consider the quantity $D_\tau = \Phi|_{t_0=0} - \Phi|_{t_0=\tau}$, where $\tau = \pi/\omega_1 = T/2$, calculated from two measurements with different values of the initial arrival time t_0. The zero-frequency component $\tilde{\phi}_0$ is removed from D_τ, and we have

$$D_\tau \propto \Re\left\{\tilde{\phi}_1\right\}, \qquad (5)$$

where we have used the fact that $\tilde{\phi}_{-k} = \tilde{\phi}_k^*$ (since ϕ is real), and where we also assumed that the phase variation is sufficiently narrowband that $\left|\tilde{\phi}_3\right| \ll \left|\tilde{\phi}_1\right|$, which will hold for a wide class of smooth phase dynamics with compact temporal support of duration $\mathcal{T} \gg T$. This shows that just two measurements with SPE states provide access to the Fourier component of a dynamical phase at a frequency $f = \omega_1/2\pi = 1/T$ fixed by the delay T between the probe photons. We note that the accuracy of this procedure is ultimately limited by the timing jitter of the nonclassical light sources that produce the photons in the SPE state, but parametric photon sources have demonstrated extremely low timing jitter[43].

1. Giovannetti, V., Lloyd, S. & Maccone, L. Quantum Metrology. *Phys. Rev. Lett.* **96**, 010401 (2006).
2. Giovannetti, V., Lloyd, S. & Maccone, L. Quantum-Enhanced Measurements: Beating the Standard Quantum Limit. *Science* **306**, 1330 (2004).
3. Boto, A. *et al.* Quantum interferometric optical lithography: Exploiting entanglement to beat the diffraction limit. *Phys. Rev. Lett.* **85**, 2733–2736 (2000).
4. Kok, P. *et al.* Quantum-interferometric optical lithography: Towards arbitrary two-dimensional patterns. *Phys. Rev. A* **63**, 063407 (2001).
5. Bollinger, J. J., Itano, W. M., Wineland, D. J. & Heinzen, D. J. Optimal frequency measurements with maximally correlated states. *Phys. Rev. A* **54**, R4649–R4652 (1996).
6. Crespi, A. *et al.* Measuring protein concentration with entangled photons. *Appl. Phys. Lett.* **100**, 233704 (2012).
7. Kimble, H. J. *et al.* Conversion of conventional gravitational-wave interferometers into quantum nondemolition interferometers by modifying their input and/or output optics. *Phys. Rev. D* **65**, 022002 (2001).
8. Aasi, J. *et al.* The characterization of Virgo data and its impact on gravitational-wave searches. *Class. Quantum Grav.* **29**, 155002 (2012).
9. Ou, Z. Y. Fundamental quantum limit in precision phase measurement. *Phys. Rev. A* **55**, 2598–2609 (1997).
10. D'Angelo, M., Chekhova, M. V. & Shih, Y. Two-photon diffraction and quantum lithography. *Phys. Rev. Lett.* **87**, 013602 (2001).
11. Walther, P. *et al.* De Broglie wavelength of a non-local four-photon state. *Nature* **429**, 158 (2004).
12. Mitchell, M. W., Lundeen, J. S. & Steinberg, A. M. Super-resolving phase measurements with a multiphoton entangled state. *Nature* **429**, 161 (2004).
13. Nagata, T. *et al.* Beating the standard quantum limit with four-entangled photons. *Science* **316** 726–729 (2007).
14. Kim, H., Park, H. S. & Choi, S.-K. Three-photon N00N states generated by photon subtraction from double photon pairs. *Opt. Express* **17**, 19720 (2009).
15. Afek, I., Ambar, O. & Silberberg, Y. High-NOON states by mixing Quantum and Classical Light. *Science* **328**, 879 (2010).
16. Thomas-Peter, N. *et al.* Real-World quantum sensors: evaluating resources for precision measurement. *Phys. Rev. Lett.* **107** 113603 (2011).
17. Greenberger, D. M., Horne, M. A. & Zeilinger, A. In *Bell's Theorem, Quantum Theory, and Conceptions of the Universe* (ed. Kafatos, M.) 73–76 (Kluwer Academic, Dordrecht, 1989).
18. Huang, Y. *et al.* Experimental generation of an eight-photon Greenberger-Horne-Zeilinger state. *Nature Commun.* **2**, 546 (2011).
19. Yao, X.-C. *et al.* Observation of eight-photon entanglement. *Nature Photon.* **6**, 225–228 (2012).
20. Kapale, K. T. & Dowling, J. P. Bootstrapping approach for generating maximally path-entangled photon states. *Phys. Rev. Lett.* **99**, 053602 (2007).
21. Dowling, J. Quantum optical metrology-the lowdown on high-N00N states. *Contemp. Phys.* **49**, 125 (2008).
22. Jacobson, J., Björk, G., Chuang, I. & Yamamoto, Y. Photonic de Broglie waves. *Phys. Rev. Lett.* **74**, 4835–4838 (2002).
23. Hong, C. K., Ou, Z. Y. & Mandel, L. Measurement of subpicosecond time intervals between two photons by interference. *Phys. Rev. Lett.* **59**, 2044 (1987).
24. Edamatsu, K., Shimizu, R. & Itoh, T. Measurement of the photonic de Broglie wavelength of entangled photon pairs generated by spontaneous parametric down-conversion. *Phys. Rev. Lett.* **89**, 213601 (2002).
25. Okamoto, R. *et al.* Beating the standard quantum limit: Phase super-sensitivity of N-photon interferometers. *N. J. Phys.* **10**, 073033 (2008).
26. Matthews, J. C. F., Politi, A., Bonneau, D. & O'Brien, J. L. Heralding two-photon and four-photon path entanglement on a chip. *Phys. Rev. Lett.* **107** 163602 (2011).
27. Holland, M. J. & Burnett, K. Interferometric detection of optical phase shifts at the Heisenberg limit. *Phys. Rev. Lett.* **71**, 1355–1358 (1993).
28. Datta, A. *et al.* Quantum metrology with imperfect states and detectors. *Phys. Rev. A* **83**, 063836 (2011).
29. Cable, H. & Dowling, J. P. Efficient generation of large number-path entanglement using only linear optics and feed-forward. *Phys. Rev. Lett.* **99**, 163604 (2007).
30. Spagnolo, N. *et al.* Polarization preserving ultra fast optical shutter for quantum information processing. *Opt. Express* **16**, 1760917615 (2008).
31. Eisaman, M. D., Fan, J., Migdall, A. & Polyakov, S. V. Invited Review Article: Single-photon sources and detectors. *Rev. Sci. Instrum.* **82**, 071101 (2011).
32. Kwiat, P. G. *et al.* New high intensity source of polarization-entangled photon pairs. *Phys. Rev. Lett.* **75**, 4337–4341 (1995).
33. Achilles, D. *et al.* Photon-number-resolving detection using time-multiplexing. *J. Mod. Opt.* **51**, 14991515 (2004).
34. Thomas, O., Yuan, Z. L. & Shields, A. J. Practical photon number detection with electric field-modulated silicon avalanche photodiodes. *Nature Commun.* **3**, 644 (2011).
35. Gerrits, T. *et al.* On-chip, photon-number-resolving, telecommunication-band detectors for scalable photonic information processing. *Phys. Rev. A* **84**, 060301 (2011).
36. Hofmann, H. F. *Phys. Rev. A* **79**, 033822 (2009).
37. Pernice, W. H. P. *et al.* High-speed and high-efficiency travelling wave single-photon detectors embedded in nanophotonic circuits. *Nature Commun.* **3**, 1325 (2012).
38. Dayan, B., Pe'er, A., Friesem, A. A. & Silberberg, Y. Nonlinear interactions with an ultrahigh flux of broadband entangled photons. *Phys. Rev. Lett.* **94**, 43602 (2005).
39. Langford, N. *et al.* Efficient quantum computing using coherent photon conversion. *Nature* **478**, 360–363 (2011).
40. Peyronel, T. *et al.* Quantum nonlinear optics with single photons enabled by strongly interacting atoms. *Nature* **488**, 57–60 (2012).
41. Ottosen, L. *et al.* Light exposure of the ovum and preimplantation embryo during ART procedures. *J. Ass. Repro. Gen.* **24** (2), 99–103 (2007).
42. Kothe, C., Björk, G. & Bourennane, M. Arbitrarily high super-resolving phase measurements at telecommunication wavelengths. *Phys. Rev. A.* **81** (6), 063836 (2010).
43. Mosley, P. *et al.* Heralded generation of ultrafast single photons in pure quantum states. *Phys. Rev. Lett.* **100**, 133601 (2008).

Acknowledgements

Author contributions

X.-M.J. and I.A.W. conceived the project and contributed to the design of the experiment. X.-M.J. and C.-Z.P. performed the experiment. M.B., J.N. contributed to the theoretical analysis. X.-M.J., Y.D., M.B., J.N. analysed the data and wrote the paper.

Additional information

How to cite this article: Jin, X.-M. *et al.* Sequential Path Entanglement for Quantum Metrology. *Sci. Rep.* **3**, 1779; DOI:10.1038/srep01779 (2013).